Materials Today Sustainability 27 (2024) 100807

Contents lists available at ScienceDirect

Materials Today Sustainability

journal homepage: www.journals.elsevier.com/materials-today-sustainability

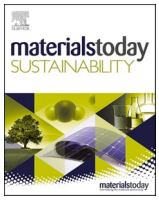

Biopolymer-derived structured graphitic carbons as metal-free heterogeneous ozonation catalysts in water

Antón López-Francés [a], Lu Peng [b], Francisco Bernat-Quesada [c], Belén Ferrer [a], Sergio Navalón [a,**], Amarajothi Dhakshinamoorthy [a,d,*], Hermenegildo García [b,***]

[a] Departamento de Química, Universitat Politècnica de València, C/Camino de Vera, s/n, 46022, Valencia, Spain
[b] Instituto de Universitario de Tecnología Química (CSIC-UPV), Universitat Politècnica de València, Av./de los Naranjos, 46022, Valencia, Spain
[c] Empresa Mixta Valenciana de Aguas SA (EMIVASA), Av. del Regne de València, 28, 46005, Valencia, Spain
[d] School of Chemistry, Madurai Kamaraj University, Madurai 625 021, Tamil Nadu, India

ARTICLE INFO

Keywords:
Heterogeneous metal-free catalysis
Carbocatalysis
Ozonation
Oxalic acid
Pollutant degradation in water

ABSTRACT

The development of metal-free heterogeneous catalysts for advanced oxidation processes is an important area of research, advancing in sustainability, with potential practical applications in water treatment. In this work, we report the development of defective structured graphitic carbons synthesized from biomass including alginate or chitosan polysaccharides and used as metal-free ozonation catalysts in water. These solids were characterized by several techniques, including powder X-ray diffraction, several spectroscopies (i.e. X-ray photoelectron, Raman or Fourier Transform infrared), elemental combustion analyses, thermogravimetric measurements, and electron microscopic techniques. The catalytic performance of graphitic carbon was examined in the ozonation reaction and the graphitic carbon derived from alginate (G) was found to be the most active catalyst by showing complete degradation in less than 4 h under the operational conditions as oxalic acid (50 mg L^{-1}), catalyst (100 mg L^{-1}), 20 °C, O_3 dosage (140 mg h^{-1}) at pH 3. Importantly, this solid retains its activity mostly upon reuse for more than 20 h, an observation that compares favorably with previous reports using graphene-based materials. In addition, activity of partially deactivated catalyst can be recovered by a pyrolysis process associated to the reconstitution of graphitic active sites of the catalyst. Experimental evidence by electron spin resonance together with specific (photo)catalytic experiments is provided to support the role of $^1O_2$ as key intermediate during the oxalic acid degradation in water in the presence of G. This study exemplifies the activity of active graphitic-based solids from biomass precursors as ozonation heterogeneous catalysts in water in the absence of any metal.

1. Introduction

Ozone (O_3) is widely used in water treatment, particularly in potable water plants, because it does not generate any residual species, while it provides some desirable properties regarding visual appearance and taste [1–3]. Although O_3 is a strong oxidizing agent ($E^o_{O3/O2} = 2.07$ V in acid media) [4], it typically requires catalysts to drive its decomposition towards the generation of the desirable reactive oxygen species (ROS) [5–7]. For this reason, the combination of O_3 with UV light or O_3 and a catalyst is considered among the most convenient advanced oxidation techniques that can be used for water remediation and pollutant degradation [8–10]. In most of the cases, transition metals, like cobalt, iron, manganese, copper, and nickel, as well as lanthanides like cerium [11] have been reported as active components in heterogeneous ozonation catalysts [12–16]. The series of these catalysts include zero-valent metals (Fe^0, Zn^0, Cu^0), metal oxides (Fe_3O_4, MnO_2, Co_3O_4) and metal/metal oxides supported on carbon-based materials (activated carbon, carbon nitrides), zeolites or silicas among other possible solids [7].

Since carboxylic acids are reluctant to undergo further oxidation under advanced oxidation techniques and these compounds are frequently the final compounds in waste water treatments, thus, they can be used as probe molecules to evaluate the activity of catalysts in advanced oxidation processes [17,18]. Specifically, we and others have used oxalic acid solutions to evaluate the catalyst performance of

* Corresponding author.
** Corresponding author.
*** Corresponding author.
E-mail addresses: sernaol@doctor.upv.es (S. Navalón), admguru@gmail.com (A. Dhakshinamoorthy), hgarcia@itq.upv.es (H. García).

https://doi.org/10.1016/j.mtsust.2024.100807
Received 13 March 2024; Received in revised form 20 April 2024; Accepted 6 May 2024
Available online 9 May 2024

carbonaceous materials in the ozonation reaction [19–26]. Since the direct decomposition of oxalic acid by O_3 in the absence of catalyst does not occur, oxalic acid disappearance rate is a simple way to determine the relative activity of various materials as ozonation catalysts against reluctant pollutants.

Graphitic carbon-based materials/composites have received significant interest in heterogeneous catalysis by employing them either as catalysts or as appropriate supports due to their salient features like structural compatibility, high surface area, pore structure and chemical-mechanical stability [27–32]. Continuing with this line of research, it would be of interest to go one step forward using metal-free catalysts for O_3 activation [32,33]. The use of carbonaceous materials as carbocatalysts has become a new topic in heterogeneous catalysis due to the clear advantages regarding sustainability that offer the use of carbon materials in comparison with transition metals [32,34–37]. Furthermore, advanced oxidation processes have been frequently attempted with commercial samples like activated carbon [38,39], graphites [40], nanographites [21], carbon nanotubes [41,42] as metal-free ozonation catalysts in water for pollutant degradation. To move further in this line of research, the originality of this work is related to the valorization of biomass waste resources (alginate or chitosan) through their transformation into graphitic carbons and to evaluate their activity towards O_3 activation for pollutant degradation in water. Therefore, our research provides new insights about the possibility of using biomass waste resources for the development of graphitic carbons as new metal free ozonation catalysts. Herein, we will present a detailed study on oxalic acid degradation in water by O_3 using various structured defective graphitic carbons synthetized from alginate (G) or chitosan polymers [(N)G]. Evidence will be shown supporting that ROS are generated on the structured G by reaction with O_3 and that subsequently these active oxygen sites promote the decomposition of oxalic acid. ROS can be determined using electron paramagnetic resonance (EPR) spectroscopy with appropriate spin traps. Further, catalyst stability is examined in terms of leaching, reusability, and productivity tests using G as a catalyst. Although the catalyst becomes deactivated upon extensive use, a facile method for the regeneration of the deactivated catalyst by thermal annealing has been developed, the regenerated catalyst being further used for another five cycles. The causes for the deactivation of the catalyst and its regeneration are proved by Raman and X-ray photoelectron spectroscopy (XPS).

2. Experimental section

2.1. Materials and reagents

Alginic acid sodium salt powder (ref. 180947), cetyltrimethylammonium chloride (CTAC, 25 wt% H_2O; ref. 292737), chitosan (CS, ref. 448,869), poly(ethylene glycol)-block-poly(propylene glycol)-block-poly(ethylene glycol) (pluronic P123; ref. 435465), dimethyl sulfoxide (DMSO, >99.9%; ref. 472,301), *tert*-butanol (>99%; ref. 360538), *p*-benzoquinone (≥98%; ref. B10358), sodium azide (NaN_3;> 99.5%; ref. S2002), 2,2,6,6-tetramethylpiperidine (TEMP; ref. 115754; ≥99%), 5,5-dimethyl-1-pyrroline N-oxide (DMPO; ref. 92688 for EPR-spectroscopy; ≥98%), cobalt (II/III) oxide (Co_3O_4; nanopowder, <50 nm particle size; ref. 637025) and multi-walled carbon nanotubes (MWCNTs; ≥98% carbon basis; ref. 773,840) were received from Merck. The rest of the chemicals employed in this work were procured from Merck with analytical or high-pressure liquid chromatography (HPLC) grade and used as received.

2.2. Preparation of G and (N)G solids

G material derived from sodium alginate was prepared as reported previously [43]. Briefly, 100 mg of sodium alginate was dissolved in 80 mL of MilliQ H_2O and stirred for 2 h at room temperature. Then, 0.4 mL 25 wt% CTAC diluted in 20 mL of Milli-Q H_2O was slowly added under magnetic stirring and was further stirred for 6 h at room temperature. The resulting mixture was subsequently submitted to hydrothermal treatment in a Teflon-lined autoclave at 100 °C for 24 h to produce structuration of sodium alginate. The templated polysaccharide precursor containing CTAC was recovered by water evaporation under reduced pressure. This solid was pyrolyzed under an Ar flow (0.5 mL min^{-1}) increasing the temperature at a rate of 5 °C min^{-1} up to 150 °C and then at 1 °C min^{-1} up to 900 °C, holding this final temperature for 2 h. During the pyrolysis, CTAC decomposes, and the byproducts evaporate, while sodium alginate is transformed into G [44].

(N)G materials having different nitrogen contents were prepared from chitosan as reported [43]. Both materials ((N)G-1 and (N)G-2) were similarly prepared only by varying Pluronic P123 and chitosan weights. To prepare (N)G-1, 34 mg of Pluronic P123 and 1.18 mL of 37 wt % hydrochloric acid were dissolved in 7.56 mL of Milli-Q H_2O at 50 °C. On the other hand, 475 mg of chitosan and 203 μL of acetic acid were dissolved in 16.25 mL of Milli-Q H_2O and subjected to magnetic stirring during 4 h. After that, the chitosan aqueous solution was added into the Pluronic P123 aqueous solution under magnetic stirring and the resulting solution stirred for 6 h at room temperature to ensure complete homogeneity. Then, the solution was placed to a Teflon-lined autoclave and heated at 100 °C under autogenous pressure for 24 h. In this hydrothermal treatment, the templation of chitosan fibrils by Pluronic P123 micelles is produced. To obtain (N)G material, the sample was pyrolyzed under Ar flow (0.5 mL min^{-1}), increasing the temperature at a rate of 2 °C min^{-1} up to 900 °C and holding the final temperature for 2 h. (N)G-2 was prepared similarly, but using 234 mg of Pluronic P123 and 325 mg of chitosan.

2.3. Catalytic activity

Catalytic ozonation experiments were carried out employing a commercial O_3 generator that provides ozonized dry air (140 mg O_3 h^{-1}; 570 mL min^{-1}) through a gas diffuser (pore size 100–160 μm) placed in the bottom of a glass reactor (500 mL). The concentration of O_3 from the generator was titrated by iodometric method. An O_3 concentration of 140 mg h^{-1} was determined for a flow of 570 mL min^{-1}, while the effective O_3 concentration present in the reaction system was estimated to be about 86.8 mg h^{-1}. For catalytic tests, G-based materials (G or (N)Gs) (100 mg L^{-1}) were dispersed by ultrasound treatment (450 W, 15 min) in an oxalic acid aqueous solution (50 mg L^{-1}, 200 mL) employing Milli-Q water. 0.1 M NaOH or 0.1 M HNO_3/HCl aqueous solution was used to adjust the pH at the required initial value. The kinetics of oxalic acid degradation was followed by analyzing periodically aliquots of the reaction mixture after filtering the suspension with a 0.2 μm Nylon filter by HPLC using a sulfonated polystyrene-divinylbenzene copolymers (ICSep ICE-COREGEL 87H3, 7.8 mm × 300 mm) column inserted in an oven (Echotherm) coupled with a UV–Vis detector. An aqueous sulfuric acid solution (0.001 N) was employed as a mobile phase at 0.8 mL min^{-1} flow rate. The catalytic experiments were carried out at least two times. The data presented corresponds to the average of each data point and the corresponding standard deviation is also presented in each figure. Additionally, the dissolved organic carbon contents of the initial and final concentration of oxalic acid previously filtrated reaction aliquots were analyzed by a High-TOC Elementar II analyzer.

Selective ROS quenching experiments were also conducted in the presence of G sample, adding 20 mol % of quencher respect to oxalic acid. DMSO and *tert*-butanol were used as HO· radical quenchers. *p*-Benzoquinone and NaN_3 were employed as selective superoxide/hydroperoxide and $^1O_2$ quenchers, respectively.

2.4. Reactivation of six-times used G as ozonation catalyst

The six-times used G (G-6U) was recovered by filtration (Nylon filter 0.22 μm) and washed three times with 1 L of Milli-Q water under stirring for 1 h each cycle, followed by drying in an oven at 100 °C for 12 h. The

dried G-6U powder was introduced in a tubular oven under Ar flow rate of 200 mL min^{-1} and heated at 900 °C at the rate of 5 °C min^{-1} with a dwelling time of 1 h. Later, the oven was cooled at room temperature while maintaining the Ar flow and the solid was washed with ethanol (100 mL) and water (100 mL), and finally dried at 100 °C for 12 h.

2.5. Characterization methods

Powder X-ray diffraction (PXRD) was measured by a Philips XPert diffractometer (40 kV and 45 mA) using Ni filtered Cu Kα radiation. UV–Vis. Raman spectra were collected at room temperature upon 315 nm laser excitation using a Renishaw in VIA Raman spectrophotometer equipped with a CCD detector. Fourier-Transform infrared (FT-IR) spectra were recorded in a Bruker spectrophotometer using an attenuated total reflectance (ATR) cell. Thermogravimetric analyses (TGA) were measured on a TGA/SDTA851e Mettler Toledo station. Isothermal N_2 adsorption measurements were performed at 77 K using Micromeritics equipment (ASAP 2010). XPS measurements were carried out with a SPECS spectrometer equipped with an MCD-9 detector using a monochromatic Al (K_α = 1486.6 eV) X-ray source. The C 1s peak at 284.4 eV was employed as reference. Combustion elemental analyses were performed using a CHNOS analyzer (PerkinElmer). Transmission electron microscopy (TEM) images of the carbonaceous samples were acquired using a field emission TEM (JEOL JEM-2100F instrument) operating at 200 kW. High resolution scanning electron microscopy (HR-SEM) images were acquired using a field emission HR-SEM (ZEISS GeminiSEM 500 instrument). EPR measurements were recorded with Bruker EMS spectrometer setting the following parameters: field 9.803 GHz, sweep width 3489.9 G, time constant 40.95 ms, modulation frequency 100 kHz, modulation width 1 G, and microwave power 19.92 mW. Zeta potential measurements were determined with a Zetasizer Nano ZS (Malvern Panalyticial UK) with 10 mg L^{-1} of G suspension with the pH range between 1 and 12 (adjusted with HCl or NaOH).

2.6. EPR measurements

EPR experiments were carried out in liquid phase using DMPO and TEMP as spin trapping agents. An aqueous solution of DMPO (1 g L^{-1}; 25 mL) with 5 mg of G solid at pH 3 were introduced in the O_3 generator for 15 min and the aliquots were sampled under identical time as shown in Fig. 4. TEMP was employed under the same conditions, but with an ozonation time of 1 min. EPR spectra of 1 mL of Ar-purged filtered aliquots (0.45 μm Nylon filter) were recorded in Bruker EMS spectrometer.

2.7. Photochemical experiments to generate $^1O_2$

Rose Bengal (50 mg L^{-1}) was used for the photochemical $^1O_2$ generation in water in the absence or presence of G (25 mg L^{-1}). A solution of oxalic acid (20 mg L^{-1}) in water at pH 3 was used as probe to determine the intrinsic activity of $^1O_2$ and $^1O_2$-activated G. Irradiation was carried out UV–Vis light from a 150 W Hg–Xe Hamamatsu L8253 lamp using a Hamamatsu spotlight source L9566-04 housing and A10014-50-0110 light guide.

3. Results and discussion

3.1. Catalyst preparation and characterization

The catalysts prepared in the present study are defective structured graphitic carbons termed as G and (N)G obtained by pyrolysis of sodium alginate or chitosan, respectively. Alginate and chitosan were previously structured by soft templation using CTAC or Pluronic 123, respectively [43–46]. Initially, these materials were characterized by powder XRD and the results are shown in Fig. 1. G exhibits a broad band centered at 2θ value of 10.92° with a d spacing of 8.1 Å, characteristic peak observed for G-based materials. Further, (N)G samples also show a broad band, but centered around 2θ value of 22° indicating higher stacking of G layers compared to G. In agreement with these observations and previous reports [43,45], a higher Brunauer–Emmett–Teller (BET) surface area and pore volume were measured for the G sample (1141 m^2 g^{-1}; 0.34 cm^3 g^{-1}) compared to (N)G-1 (384 m^2 g^{-1}; 0.073 cm^3 g^{-1}) or (N)G-2 (443 m^2 g^{-1}; 0.088 cm^3 g^{-1}) (Fig. 1).

The graphitic nature of these samples was confirmed by Raman spectroscopy (Fig. S1). Raman spectroscopy is a common

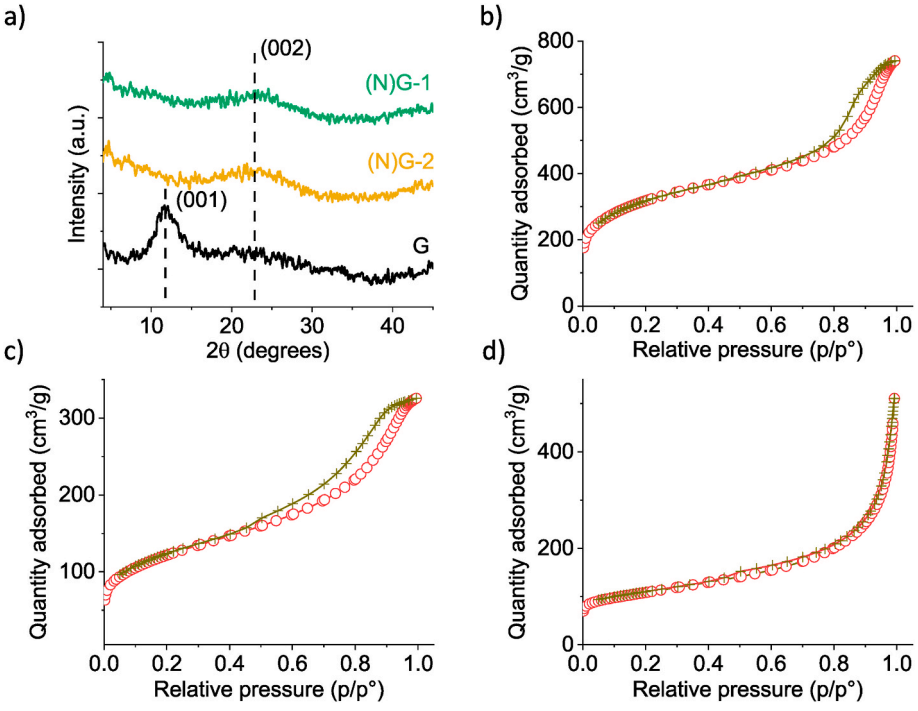

Fig. 1. a) Powder XRD and BET surface area of b) G, c) (N)G-1 and d) (N)G-2 materials.

characterization tool to determine the degree of defects in carbon-based materials, including graphites, graphenes and hybridized sp^2/sp^3 carbons, among others [32]. In general, the so-called G band is related to the presence of ideal graphitic domains on a carbon material, while the D band is related with the presence of structural defects, like the presence of heteroatoms such as oxygen or nitrogen. Fig. 2a shows the expected G and broad D vibration bands at 1590 and 1350 cm^{-1} for G, (N)G-1 and (N)G-2 solids, accompanied by a harmonic band at about 2950 cm^{-1} corresponding to the G + D harmonic frequency. Raman spectra can be also used to determine I_D/I_G intensity ratio that is often used as a semiquantitative parameter to rank the degree of defects on carbon-based materials, the higher the I_D/I_G value, the higher the number of defects within the sample. In the present case, the level of disorder in these samples was also evaluated from the ratio I_D/I_G ratio (Fig. 2a), the lower ratio observed for G associated is proposed to be associated with a higher graphitic nature of this sample.

Elemental combustion analyses confirmed the presence of carbon and nitrogen elements in (N)G-1 (74.5 wt% C and 4.6 wt% N) and (N)G-2 (72.1 wt% C and 2.4 wt% N) ascribed to the presence of amino groups in chitosan polymer precursor employed during the synthesis of these solids. In the case of G, carbon was the main element (80.5 wt% C), but it was also accompanied by nitrogen atoms (2 wt%) and it is attributed to the incomplete removal of CTAC used as templating agent during the pyrolysis treatment.

XPS analyses were further employed to determine the chemical nature of carbon and nitrogen elements, together with oxygen atoms (Fig. 2b–d, Figs. S2–S4 and Table S1) [47]. In general, the three G-based materials are characterized by a XPS C 1s spectra with a main band centered at 284.4 eV due to sp^2 carbons accompanied with other bands at ~285 eV due to C–O/C–OH/C–N bonds, at ~288 eV associated to carbonyl groups, ~290 eV characteristic of carboxylate derivatives, while the band at about ~291.5 eV due to π-π* transition of carbon in aromatic moieties. XPS O 1s level shows three bands associated with carbonyl/quinone (~530 eV), hydroxyl/ether (~532 eV) or carboxylic acid/lactones (~534 eV). In the case of (N)G samples, N 1s bands are attributed to graphitic (402 eV) and amino groups (399 eV), while G sample shows the presence of a main component of graphitic nitrogen.

FT-IR spectroscopy was also employed to monitor the changes of surface functional groups present in the different types of graphitic carbon materials (Fig. S5). FT-IR spectrum of G shows the presence of weak bands associated to hydroxyl groups (3420 cm^{-1}), which are not present or seen in lower intensity in (N)G-based samples. The weak bands at about 2970 and 2890 cm^{-1} in the FT-IR spectra of N(G) solids are characteristic for asymmetric and symmetric –CH_2- stretching vibrations, respectively. FT-IR spectra of G and (N)G have some bands around 1600 and 1500 cm^{-1} which are due to aromatic C=C stretching vibrations. The broad band centered at 1100 cm^{-1} can be assigned to vibrations of C–O and C–N bonds.

HR-SEM and HR-TEM measurements revealed the presence of tubular-like morphologies generated in the soft templation step of sodium alginate followed by graphitization (Fig. 3). Similar characterization analyses for (N)G-1 and (N)G-2 solids revealed the presence of graphitic carbon layers with an interlayer distance of 0.38 nm which is a typical value for graphene-based materials.

To put into context the catalytic activity of G and (N)G solids, other materials were also considered in this study. The list of materials includes commercial Co_3O_4 nanoparticles (NPs) (<50 nm size; 40–70 m^2 g^{-1}) since it is one of the most active transition metals for O_3 activation [12,13]. Commercial MWCNTs (3–6 μm size; 280–350 m^2 g^{-1}) containing some Fe impurities (Fe percentage in MWCNTS obtained by ICP-OES ~ 0.01 wt%) were also used as control to compare the performance of G and (N)G catalysts.

3.2. Catalytic activity

The catalytic performance of the as-prepared solids as ozonation catalysts was carried out in aqueous suspension, bubbling continuously O_3 (140 mg h^{-1}) through an aqueous solution of oxalic acid (50 mg L^{-1}) at room temperature at pH 3. Fig. 4 shows the temporal profile of oxalic acid decomposition in the presence of various catalysts under evaluation. As expected, in the absence of any catalyst, oxalic acid concentration by direct reaction with O_3 decreased less than 10 % after 5 h. Besides, control experiments revealed that oxalic acid removal by adsorption on G is lower than 5 % after 5 h. The presence of (N)G-1 increased oxalic acid degradation marginally to 15 % after 5 h. The other samples under study were significantly more efficient although (N)G-2 was a less active sample compared to commercial samples of Co_3O_4 NPs and MWCNTs. In contrast, G exhibits a remarkable activity, close to that

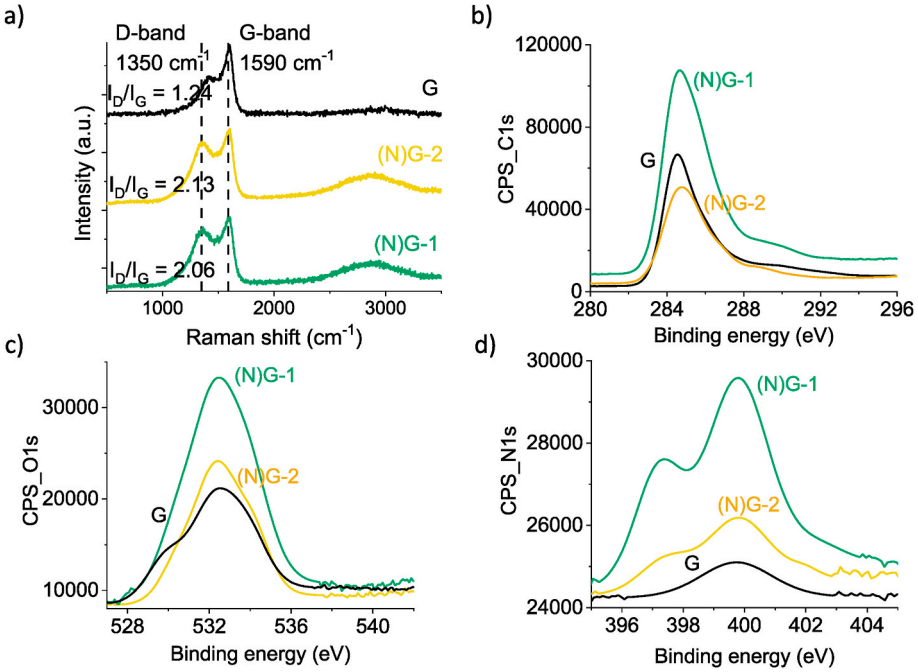

Fig. 2. a) Raman spectra of G, (N)G-1, (N)G-2 and high-resolution XPS of b) C 1s, c) O 1s, d) N1s for G, (N)G-1, (N)G-2 materials.

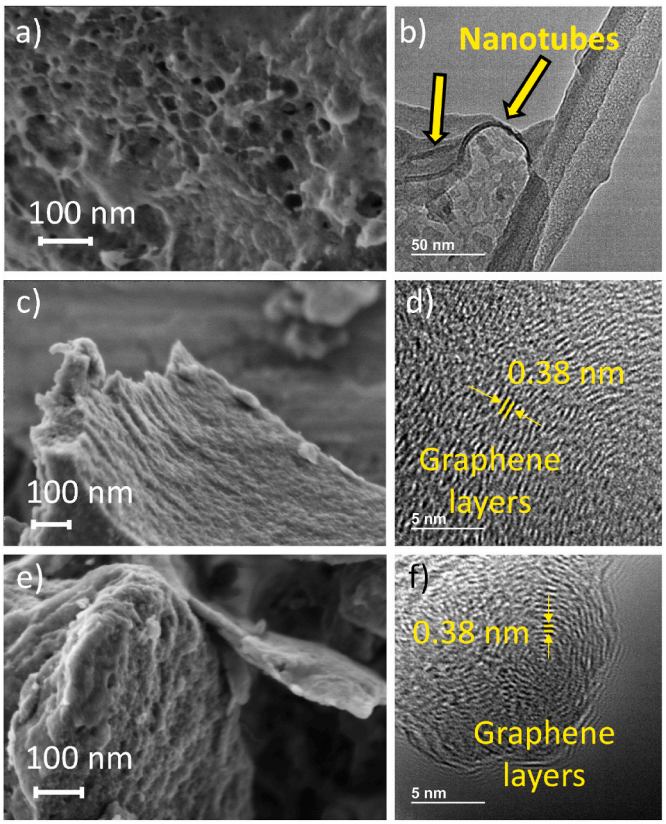

Fig. 3. HR-SEM images of a) G, c) (N)G-1 and e) (N)G-2 and HR-TEM images of b) G, d) (N)G-1 and f) (N)G-2 solids.

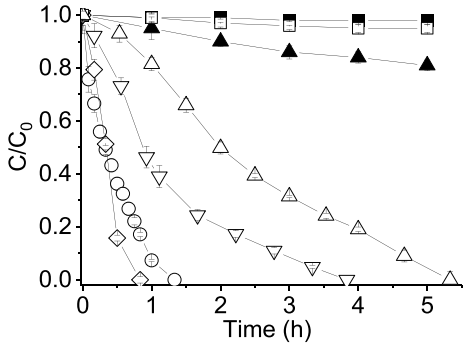

Fig. 4. Comparison of the catalytic activity of a series of catalysts for ozonation reaction, using oxalic acid in water at pH 3. Legend: O_3 (■), adsorption of oxalic acid on G without O_3 (□), ozonation in the presence of catalysts: (N)G-1 (▲), (N)G-2 (△), G (▽), Co_3O_4 NPs (○) and MWCNTs (◇). Reaction conditions: oxalic acid (50 mg L^{-1}), catalyst (100 mg L^{-1}), 20 °C, O_3 inlet (not for adsorption experiment, □) into the glass reactor (140 mg h^{-1}).

of Co_3O_4 NPs and MWCNTs as reference catalysts, achieving a complete oxalic acid degradation in less than 4 h. The lower catalytic activity of (N)Gs compared to G can be associated to their reluctance to undergo oxidation by O_3 and the lack of activity to form ROS which are able to degrade oxalic acid. The results presented in Fig. 4 clearly show the notable ozonation activity of G as a metal-free catalyst. Further, complete oxalic acid mineralization was assessed with G as the catalyst by measuring the dissolved organic carbon of the samples previously filtered at the initial and at the final reaction time.

The pH value of the reaction medium has a remarkable influence in the generation of ROS and hence, oxalic acid degradation was also optimized at different pH values in the range from 3 to 9 using either HNO_3 or NaOH. In a control experiment, to figure out the potential oxidizing effect of NO_3^- ions under acidic conditions in the catalytic ozonation process, the performance of G as a catalyst at pH 3 using HCl was performed under identical conditions as shown in Fig. 5 and observing similar degradation kinetics. Fig. 5 shows that the catalytic activity of G decreased as the pH value of the medium is increased. This observation might be attributed to the lower stability of O_3 in water at basic pH values [20,48] that results in lower available amount of O_3 to be catalytically transformed into active ROS. Besides considering the stability of O_3, previous studies have proposed that the inherent properties of the catalyst such as its point of zero charge (PZC) can influence the catalytic efficiency as a function of the pH of the solution [49–51]. In the present case, the influence of the pH on a G water suspension on the resulting Zeta potential was measured and the results are shown in Fig. S11. From these data the PZC was estimated to be 2.47. Then, oxalic acid adsorption on G suspensions at different pH values was studied. The results indicated that oxalic acid adsorption on G gradually decreases (*ca* 5 wt% adsorption at pH 3) as the pH increases (*ca* 1 wt% adsorption at pH 9). These results were rationalized considering that basic pH values result in negative PZC of G and, thus, oxalate adsorption is unfavorable due to repulsion of negative charges between them. Therefore, the higher oxalic acid adsorption and O_3 stability observed at acidic pH values can favor the catalytic degradation of oxalic acid in water. In the area of heterogeneous catalytic ozonation for pollutant degradation in water, some studies have proposed that this process is more efficient at pH values close to the PZC [50,52] and a similar situation might also occur in the present case.

One important point in heterogeneous catalysis is to show that the reaction occurs on the solid surface and not in solution due to the leaching of some active species. Heterogeneity is typically proved by performing twin experiments, removing in one of them the solid catalyst at a certain reaction time after some product evolution has occurred and observing that the reaction stops after solid removal. The results of the leaching experiment are presented in Fig. 6. As can be seen there, the three initial points at 0, 10 and 40 min of the two experiments coincide for the twin reactions. However, oxalic acid continues disappearing in the presence of G as catalyst and it becomes completely degraded after 230 min. In contrast, degradation of oxalic acid completely stops upon removal of G by filtration under similar conditions. This experiment convincingly proves that oxalic acid degradation is only possible with the assistance of G as the catalyst and further no leaching of active sites occurs to the solution. This is important information since ROS, particularly O_3 and other species derived therefrom, must be present in the liquid phase as short- or long-lived compounds. However, this cocktail of ROS in solution is completely inefficient to degrade oxalic acid under the current experimental conditions as shown in Fig. 6. This filtration test proves that the presence of G as the catalyst is essential for oxalic acid degradation.

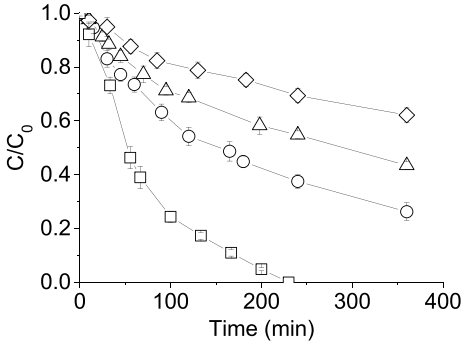

Fig. 5. Carbocatalytic ozonation of oxalic acid at different initial pH values using G. Legend: pH 3 (□), pH 5 (○), pH 7 (△) and pH 9 (◇). Reaction conditions: oxalic acid (50 mg L^{-1}), G (100 mg L^{-1}), 20 °C, O_3 inlet into the glass reactor (140 mg h^{-1}).

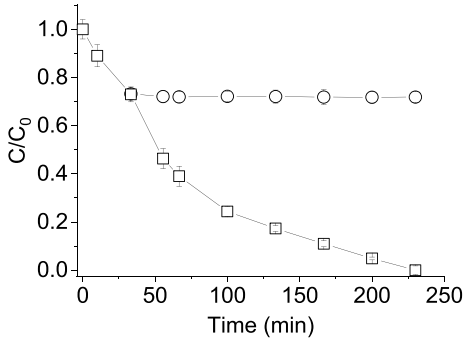

Fig. 6. Oxalic acid degradation in the presence of G (□) or starting the reaction in the presence of G that was filtered at 40 min (○). Reaction conditions: oxalic acid (50 mg L^{-1}), G (100 mg L^{-1}), pH 3, 20 °C, O_3 inlet to the glass reactor (140 mg h^{-1}).

Assessment of catalyst stability in subsequent cycles is one of the important aspects to be addressed in heterogeneous catalysis. To determine the stability of G, this solid was used in a series of six consecutive ozonation reactions. The results are presented in Fig. 7a. It was observed that the material exhibited a gradual decrease in its catalytic activity. Six-times used G (G-6U) sample exhibited only 40 % degradation efficiency compared to the 100 % degradation achieved by the fresh G sample under similar experimental conditions. In addition, the somewhat slower initial reaction rate was measured for G-6U solid in comparison to the fresh G sample. On the other hand, G was also used as a metal-free catalyst for the productivity test for the degradation of a relatively large amount of oxalic acid (1 g L^{-1}) in water at pH 3 as shown in Fig. 7b. These results are highly promising considering that oxalic acid is completely degraded after 225 h suggesting the durability of G as solid heterogeneous catalyst.

Based on these observations and previous related precedents [19, 20], we postulate that this activity decay should be due to the partial G oxidation with concomitant decrease in the population of active sites. It should be noted that sp^2 aromatic carbon edges have been proposed as active sites for O_3 activation. To address this hypothesis, Raman spectroscopy was used to characterize the possible changes that occurred with G solid during the catalytic ozonation reuse experiments (Figs. 8a and S6). G-6U sample shows a higher number of defects (I_D/I_G ratio 1.32) compared to the fresh sample (I_D/I_G ratio 1.24) as shown in Fig. 8a. It is likely that these defects are related to the presence of oxygen functional groups on the G sample due to its partial oxidation during the catalytic ozonation. Interestingly, thermal annealing of G-6U solid under Ar atmosphere (900 °C for 1 h) was performed to reduce the number of defects (G-6U-REG) and its I_D/I_G ratio (1.15) is measured to be close to fresh G solid.

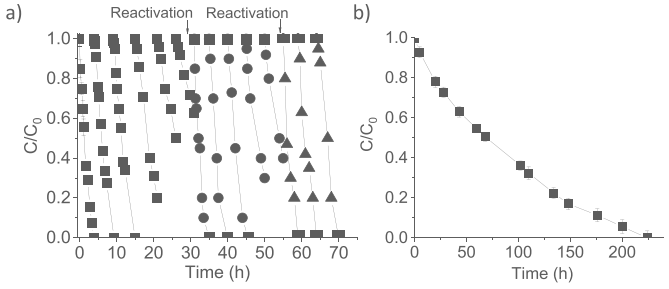

Fig. 7. a) Reusability study and the influence of the thermal reactivation at 900 °C for G as a metal-free catalyst during the ozonation of oxalic acid at pH 3. Reaction conditions: Carbocatalyst (100 mg L^{-1}), oxalic acid (50 mg L^{-1}), temperature 20 °C, O_3 inlet to the glass reactor (140 mg h^{-1}). b) Productivity test for the degradation of a relatively large amount of oxalic acid (1 g L^{-1}) in water at pH 3 using G at 50 mg L^{-1} catalyst (■).

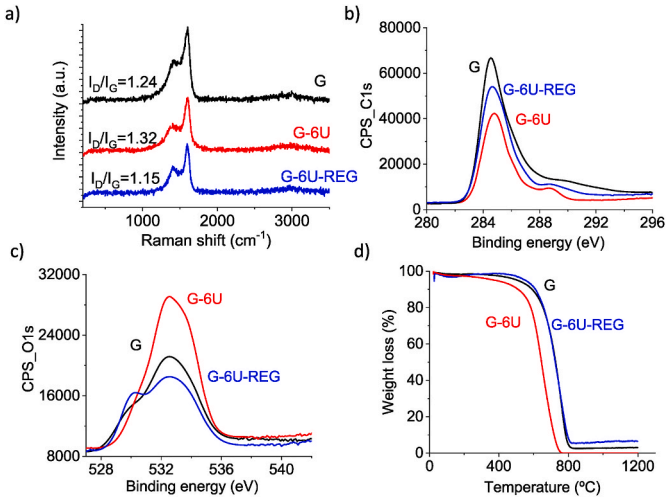

Fig. 8. a) Raman spectroscopy with indication of I_D/I_G ratio, b) XPS C 1s, c) XPS O 1s, and d) TGA of G, G-6U and G-6U-REG. G-6U and G-6U-REG refer to the six times used G and the regenerated sample by pyrolysis, respectively.

XPS analyses were also carried out to gain some information about the structural properties of partially deactivated (G-6U) and regenerated (G-6U-REG) samples (Fig. 8 and Figs. S7–S9). The observed changes in XPS C 1s spectra are compatible with the partial oxidation of G during the catalytic ozonation as revealed by a decrease of the π-π* band intensity (~290.5 eV) in the G-6U. Interestingly, this band is recovered in G-6U-REG sample. In addition, XPS O 1s clearly revealed an increase of oxygen functional groups (16.4 at%) of G-6U compared to fresh G sample (12.9 at%), while G-6U-REG sample recovers the initial composition of oxygen functionalities (13.7 wt%) (Table S2). Detailed XPS analyses revealed that graphitic carbon of G-6U is carbonyl/quinone (~530.7 eV), hydroxyl/ether (~532.1 eV) or carboxylic acid/lactones (~533.3 eV). Additionally, the functional groups present in G-6U-REG are identical to fresh G, except for the presence of additional carbonyl/quinone (~530.7 eV) groups. In the case of N 1s, no significant observable changes of graphitic nitrogen were observed.

Furthermore, FT-IR spectra (Fig. S10) indicate that the relative intensities of O–H (3300 cm^{-1}) and C=O (1710 cm^{-1}) stretching vibrations in G-6U solid slightly increased compared to fresh G and this is associated to the introduction of alcohols and/or carbonyl/carboxylate-like groups. In contrast, FT-IR spectrum of the G-6U-REG solid resembles identical to that of fresh G, due to the removal of oxygen functionalities through pyrolysis. In agreement with these observations, G-6U sample exhibits lower thermal stability than G due to the presence of unstable oxygen-functional groups such as carboxylates from about 400 °C [53], while G-6U-REG recovers the thermal stability equivalent to G.

To further confirm the physicochemical properties of G during the reusability study, HR-TEM measurements for G, G-6U and G-6U-REG samples were performed and their images along with the d-spacing values are presented in Figs. S12 and S13. These HR-TEM images confirm that the partial deactivation of G is due to the oxidation of the graphitic structure (G-6U) and this issue can be solved by pyrolysis to regenerate the catalyst through re-graphitization (G-6U-REG). In other words, G and G-6U-REG are characterized by graphitic domains with sp^2 C–C bonds having d-spacings of about 0.35 nm while G-6U have in addition d-spacings of about 0.23 nm associated with sp^3 C–C bonds (Fig. S13). These results are in good agreement with previous XPS, Raman and TGA measurements.

The achieved catalytic data indicate that G solid is an active metal-free carbon-based material that can be reused five times, while retaining about 70 % of its initial activity (Fig. 7a). To put into context these results, Table 1 summarizes the activity and stability of some previously reported graphitic materials as heterogeneous ozonation catalysts in

Table 1
Comparison of the catalytic activity of G with previous related studies using graphene materials. rGO corresponds to reduced graphene oxide.

Catalyst	Reaction conditions	General remarks	Ref.
rGO	Catalyst (50 mg L^{-1}), oxalic acid aqueous solution (50 mg L^{-1}), O_3 (140 mg h^{-1}), pH 3, 20 °C, 120 min	The activity of rGO decreases about 80 % after its first use	[54]
rGO	Catalyst (100 mg L^{-1}), *p*-hydroxybenzoic acid aqueous solution (20 mg L^{-1}), O_3 (100 mL min^{-1}; 20 mg L^{-1}), 25 °C, 30 min	The activity of fresh catalyst decreases more than 40 % of initial activity after its first use	[55]
Hybrid sp^2/sp^3 nanodiamonds	Catalyst (100 mg L^{-1}), oxalic acid aqueous solution (50 mg L^{-1}), O_3 (140 mg h^{-1}), pH 3, 20 °C, 180 min	The catalyst loses more than 50 % of its initial catalytic activity after its first use	[19]
N-rGO	Catalyst (250 mg L^{-1}), benzotriazole (0.084 mM), O_3 (2 mg L^{-1}), pH 4.75, 7.5 min	The catalyst partially deactivates upon reuse and requires an increase of reaction time from 7.5 to 30 min to achieve similar conversion.	[56]
rGO	Catalyst (100 mg L^{-1}), 4-nitrophenol (50 mg L^{-1}), O_3 (100 mL min^{-1}; 50 mg L^{-1}), pH 5, 25 °C	The catalyst partially deactivates upon reuse resulting in an increase of the reaction time to 20 and 30 min to achieve full conversion compared to the fresh sample (15 min)	[57]
N-rGO	Catalyst (100 mg L^{-1}), 4-nitrophenol (50 mg L^{-1}), O_3 (100 mL min^{-1}; 50 mg L^{-1}), pH 5, 25 °C	The catalyst partially deactivates about 22 % after its third use.	[58]

water. A general conclusion from these previous studies indicates that single or few layers graphene materials or hybrid sp^2/sp^3 nanodiamonds are active ozonation catalysts that suffer strong deactivation after their first use. Therefore, it is believed that the G solid prepared in this work exhibits improved stability compared to previous single or few layers graphene-based ozonation catalysts.

3.3. Reaction mechanism

Control experiments shown in Fig. 4 indicate that oxalic acid degradation does not occur in the absence of O_3 or G, which are in good agreement with the previous reports that has proposed oxalic acid as probe for catalytic ozonation reaction. To gain some insights into the reaction mechanism and to identify the formation of ROS, EPR measurements and quenching experiments were carried out. The presence of ROS in solution was confirmed by EPR spectroscopy by performing an ozonation experiment in the presence of G under optimized conditions for short reaction times, but in the presence of spin traps. For this purpose, two spin trap agents, namely DMPO and TEMP were used to trap selectively $HO^{\cdot}/HOO\cdot/O_2^{\cdot-}$ radicals and $^1O_2$, respectively. In these trapping experiments, EPR spectroscopy was able to determine the corresponding expected trapping adducts, mainly DMPOX and TEMPO (Fig. 9). Specifically, EPR experiment using TEMP as a spin trap confirms the catalytic O_3 transformation into $^1O_2$, while the EPR measurement with DMPO excludes the formation of $HO\cdot/HOO\cdot/O_2^{\cdot-}$ radicals. The presence of a characteristic peak pattern for DMPOX is due to the oxidation of DMPO, either by O_3 [59] or $^1O_2$ [60,61], as previously reported.

To further validate the formation of ROS during the catalytic ozonation involving G as the catalyst, quenching experiments were performed using selective quenchers. In these quenching studies, oxalic acid degradation should stop when the reaction is performed in the

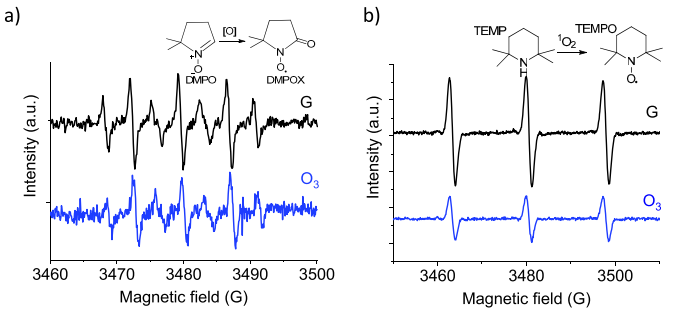

Fig. 9. EPR spectra recorded at short ozonation time (10 min) using G as a metal-free catalyst in the presence of a) DMPO and b) TEMP as spin trapping agents.

presence of a quencher for a specific ROS that plays a role as active species. Fig. 10a–c shows the temporal profile of oxalic acid degradation using G as the catalyst in the presence of different quenchers and concentrations (*ca* 1, 10 and 20 mol % quencher respect to oxalic acid). As it can be seen there, oxalic acid degradation is not affected by the presence of *p*-benzoquinone that is a quencher for $O_2^{\cdot-}/HOO\cdot$ or *tert*-butanol for $HO\cdot$ radicals. In fact, previous studies have reported the rate constants for the reaction between these quenchers and the ROS. For instance, *tert*-butanol was used as quencher for $HO\cdot$ radical quenching in solution resulting in a rate constant with the value of 5×10^8 $M^{-1}s^{-1}$ [62]. It should be noted that the reactivity of O_3 with *tert*-butanol is almost negligible (3×10^{-3} $M^{-1}s^{-1}$) compared to the reactivity of $HO\cdot$ radicals. Interestingly, the quenching effect of NaN_3 on oxalic acid degradation during the catalytic ozonation using G increases along its concentration (*ca* 1, 10 and 20 mol % respect to oxalic acid). Previous reports have described that the quenching of $^1O_2$ by NaN_3 occurs through the formation of a partial charge-transfer intermediate ($N_3^- + {}^1O_2 \rightarrow [N_3\cdots O_2^-]$ [63]. These results are in agreement with EPR measurements, but somehow surprising and unexpected, since oxalic acid degradation by catalytic ozonation is mostly occurring through $HO\cdot$ radicals and not by

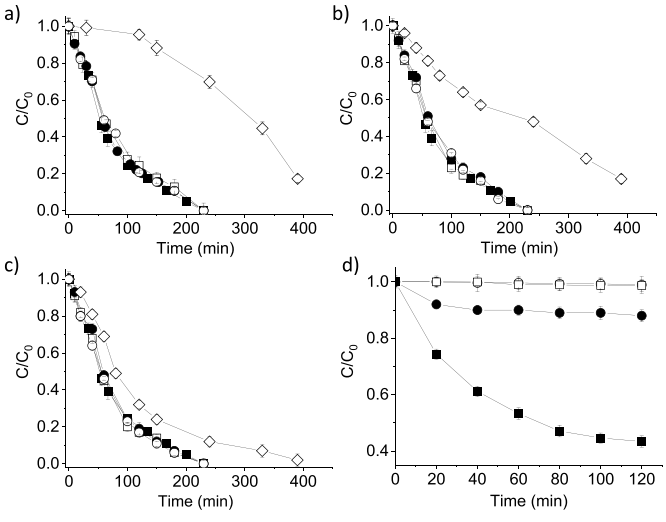

Fig. 10. Carbocatalytic ozonation of oxalic acid at pH 3 using G as carbocatalyst in the absence (■) or in the presence of NaN_3 (◇), DMSO (●), *tert*-butanol (□) and *p*-benzoquinone (○) at a) 20 mol%, b) 10 mol% and c) 1 mol%. Reaction conditions: oxalic acid (50 mg L^{-1}), G (100 mg L^{-1}), 20 °C, O_3 inlet to the glass reactor (140 mg h^{-1}). d) Metal-free catalytic degradation of oxalic acid in water at pH 3 using G and Rose Bengal. Legend: oxalic acid solution and absence of both Rose Bengal and G (○); oxalic acid solution irradiating with Rose Bengal in the absence of G (□); irradiating with Rose Bengal and G (250 mg L^{-1}) for 60 min, lights off and, then, addition of oxalic acid (●); oxalic acid solution irradiating with Rose Bengal and G (100 mg L^{-1}) (■). Reaction conditions: Rose Bengal (50 mg L^{-1}), oxalic acid (20 mg L^{-1}), 20 °C.

HOO· radicals [32]. These results imply that somehow $^1O_2$ is the main ROS responsible for oxalic acid degradation in the presence of G under the present experimental conditions.

To understand better the role of $^1O_2$ as the ROS in the degradation of oxalic acid, three additional and complementary reactions were carried out. The results are presented in Fig. 10d. In one of these experiments to understand the role of $^1O_2$, degradation of oxalic acid was attempted in the absence of O_3 by irradiation of the aqueous solution of Rose Bengal as $^1O_2$ photosensitizer with UV–Vis. No oxalic acid degradation was observed under these conditions, meaning that $^1O_2$ in homogeneous phase is unable to degrade oxalic acid, a fact that is in agreement with the prior assumption that oxalic acid degradation is specific to HO· radicals. In a second experiment, visible light illumination of Rose Bengal was performed in the presence of G as the catalyst. Degradation of oxalic acid under these conditions was observed, meaning that the combination of $^1O_2$ with G as the catalyst generates active sites to decompose oxalic acid. In the third experiment, a larger-than-usual amount of G (250 mg L^{-1} rather than 100 mg L^{-1}) was submitted to $^1O_2$ for 60 min by irradiation of Rose Bengal in the absence of oxalic acid and after this time, the light was switch off and oxalic acid was added in the absence of $^1O_2$ generation. Oxalic acid degradation was observed under these conditions in which no direct contact between $^1O_2$ and G has taken place, meaning that it is the G surface attacked by $^1O_2$ what causes oxalic acid decomposition. Of note is that the amount of G present in the system is limited by the constraints of the photochemical $^1O_2$ generation that requires certain transparency to Rose Bengal excitation. Importantly, if instead of Rose Bengal irradiation, G is exposed to O_3 in the absence of oxalic acid and subsequently, ozonation is discontinued and oxalic acid is added, similar results as those observed for Rose Bengal were achieved and oxalic acid degradation proceeds in the absence of O_3 flow.

To reconcile all the results, particularly the main role of $^1O_2$ as responsible for oxalic acid degradation and the fact that in the absence of G, $^1O_2$ is unable to attack oxalic acid, it is proposed that $^1O_2$ reacts with G forming the real active species that are efficient to degrade oxalic acid. These surface reactive species do not require further $^1O_2$ to attack oxalic acid and for this reason the reaction can be performed sequentially as observed in Fig. 10d. This proposal agrees with the prior ozonation observation that removal of G completely stops oxalic acid degradation (Fig. 6) suggesting that none of the ROS in solution decomposes oxalic acid or the Rose Bengal photosensitized $^1O_2$ generation that also fails to decompose oxalic acid in the absence of G.

Based on the known reactivity of $^1O_2$ and the fact that it readily reacts with condensed polycyclic aromatic compounds, such as anthracene to form endoperoxides and, also knowing the mechanistic decomposition of these aromatic endoperoxides [64,65]. It is proposed that $^1O_2$ reacts initially with polyaromatic rings present in G to form aromatic endoperoxides. The lower catalytic activity of (N)G can be rationalized accordingly due to their reluctance to undergo oxidation compared to analogous N-free carbons. These aromatic endoperoxides are reasonable stable in acidic conditions but degrade catalytic in the presence of bases. Therefore, at acidic pH and ambient temperatures, these endoperoxides should survive for a certain time. Acid catalyzed decomposition of surface generated endoperoxide can generate oxyl radicals that, although less reactive than HO· radicals are proposed to attack oxalic acid and promote its decomposition.

4. Conclusions

Catalytic ozonation is an established process to increase O_3 activity in degradation processes of organic compounds. Most of the reported ozonation catalysts are based on transition metals as the most efficient catalysts for O_3 activation. In these cases, the main involved ROS are HO· radicals and oxalic acid has been proposed as a suitable probe to determine catalyst perfoemance for O_3 activation. Herein, we have shown that metal-free structured G synthesized from biopolymers such as alginate or chitosan can be employed as ozonation catalysts. Among these catalysts, G exhibited 100% degradation of oxalic acid in less than 4 h which is far better than (N)G-1 (20%) and (N)G-2 (100% after 5.5 h) catalysts under the operational conditions as oxalic acid (50 mg L^{-1}), catalyst (100 mg L^{-1}), 20 °C, O_3 dosage (140 mg h^{-1}). Interestingly, productivity test using G as catalyst shows the complete removal of oxalic acid (1 g L^{-1}) after 225 h suggesting the durability of G under the present operational conditions. Further, the performance of G as the ozonation catalyst for the degradation of oxalic acid involves $^1O_2$, a fact that is remarkable considering the sustainability in the preparation of G. The reaction does not involve a radical chain reaction in the liquid phase but occurs in the presence of G previously treated either with $^1O_2$ or O_3. Characterization of the partially deactivated G-6U sample during the consecutive six reuses indicates that deactivation appears to be caused by G oxidation. This partial oxidation can be completely reverted by pyrolysis, restoring its structural integrity and catalytic activity as equivalent to the fresh material. Quenching and spin trap experiments with EPR spectroscopy confirmed the involvement of $^1O_2$ as key ROS under the optimized experimental conditions. Overall, the present study unambiguously proves the active role played by $^1O_2$ as ROS in ozonation using metal-free carbonaceous materials from sustainable biopolymers.

CRediT authorship contribution statement

Antón López-Francés: Investigation. **Lu Peng:** Investigation. **Francisco Bernat-Quesada:** Methodology. **Belén Ferrer:** Investigation. **Sergio Navalón:** Writing – original draft, Supervision, Conceptualization. **Amarajothi Dhakshinamoorthy:** Writing – review & editing, Writing – original draft, Supervision. **Hermenegildo García:** Writing – review & editing, Writing – original draft, Methodology.

Declaration of competing interest

The authors declare that they have no known competing financial interests or personal relationships that could have appeared to influence the work reported in this paper.

Data availability

Data will be made available on request.

Acknowledgements

S.N. thanks the support received from Grant PID2021–123856OB-I00 funded by MICIU/AEI/10.13039/501100011033 and by ERDF A way of making Europe. A.D. is beneficiary of a grant María Zambrano in Universitat Politècnica de València within the framework of the grants for the retraining in the Spanish university system (Spanish Ministry of Universities, financed by the European Union, NextGeneration EU). H.G. thanks the financial support by the Spanish Ministry of Science and Innovation (CEX-2021-001230-S and PDI2021-0126071-OB-CO21 funded by MICIU/AEI/10.13039/501100011033) and Generalitat Valenciana (Prometeo 2021/038 and Advanced Materials programme Graphica MFA/2022/023 with funding from European Union NextGenerationEU PRTR-C17. I1). Funding for open access charge: CRUE-Universitat Politècnica de València.

Appendix A. Supplementary data

Supplementary data to this article can be found online at https://doi.org/10.1016/j.mtsust.2024.100807.

References

[1] J. Lawrence, F.P. Cappelli, Ozone in drinking water treatment: a review, Sci. Total Environ. 7 (1977) 99–108.

[2] V. Camel, A. Bermond, The use of ozone and associated oxidation processes in drinking water treatment, Water Res. 32 (1998) 3208–3222.
[3] B.L. Loeb, C.M. Thompson, J. Drago, H. Takahara, S. Baig, Worldwide ozone capacity for treatment of drinking water and wastewater: a review, Ozone: Sci. Eng. 34 (2012) 64–77.
[4] F.J. Beltrán, Ozone-UV radiation-hydrogen peroxide oxidation technologies, Environ. Sci. Pollut. Control Ser. (2003) 1–76.
[5] B. Liu, J. Ji, B. Zhang, W. Huang, Y. Gan, D.Y.C. Leung, H. Huang, Catalytic ozonation of VOCs at low temperature: a comprehensive review, J. Hazard. Mater. 422 (2022) 126847.
[6] E. Issaka, J.N. Amu-Darko, S. Yakubu, F.O. Fapohunda, N. Ali, M. Bilal, Advanced catalytic ozonation for degradation of pharmaceutical pollutants-a review, Chemosphere 289 (2022) 133208.
[7] W. Chen, H. He, J. Liang, X. Wei, X. Li, J. Wang, L. Li, A comprehensive review on metal based active sites and their interaction with O3 during heterogeneous catalytic ozonation process: types, regulation and authentication, J. Hazard. Mater. 443 (2023) 130302.
[8] C.V. Rekhate, J.K. Srivastava, Recent advances in ozone-based advanced oxidation processes for treatment of wastewater-A review, Chem. Eng. J. Adv. 3 (2020) 100031.
[9] K. Ikehata, M. Gamal El-Din, Aqueous pesticide degradation by ozonation and ozone-based advanced oxidation processes: a review (Part I), Ozone: Sci. Eng. 27 (2005) 83–114.
[10] A. Al-Kdasi, A. Idris, K. Saed, C.T. Guan, Treatment of textile wastewater by advanced oxidation processes—a review, Global Nest: Int. J. 6 (2004) 222–230.
[11] C.A. Orge, J.J.M. Órfão, M.F.R. Pereira, A.M.F. Duarte de FariasM.A., Ceria and cerium-based mixed oxides as ozonation catalysts, Chem. Eng. J. 200–202 (2012) 499–505.
[12] P. Konova, M. Stoyanova, A. Naydenov, D. Mehandjiev, Catalytic oxidation of VOCs and CO by ozone over alumina supported cobalt oxide, Appl. Catal., A 298 (2006) 109–114.
[13] L. Zhang, F. Huo, A. Wang, S. Chai, J. Guan, G. Fan, W. Yang, G. Ma, N. Han, Y. Chen, Coordination-controlled catalytic activity of cobalt oxides for ozone decomposition, Inorg. Chem. 62 (2023) 9178–9189.
[14] Y. Qi, C. Guo, X. Xu, B. Gao, Q. Yue, B. Jiang, Z. Qian, C. Wang, Y. Zhang, Co/Fe and Co/Al layered double oxides ozone catalyst for the deep degradation of aniline: preparation, characterization and kinetic model, Sci. Total Environ. 715 (2020) 136982.
[15] T. Batakliev, V. Georgiev, M. Anachkov, S. Rakovsky, G.E. Zaikov, Ozone decomposition, Interdiscipl. Toxicol. 7 (2014) 47–59.
[16] X. Li, J. Ma, H. He, Recent advances in catalytic decomposition of ozone, J. Environ. Sci. 94 (2020) 14–31.
[17] K. Ikehata, M.G. El-Din, Degradation of recalcitrant surfactants in wastewater by ozonation and advanced oxidation processes: a review, Ozone: Sci. Eng. 26 (2004) 327–343.
[18] M.A. Oturan, J. Aaron, Advanced oxidation processes in water/wastewater treatment: principles and applications. A review, Crit. Rev. Environ. Sci. Technol. 44 (2014) 2577–2641.
[19] F. Bernat-Quesada, C. Valles-Garcia, E. Montero-Lanzuela, A. López-Francés, B. Ferrer, H.G. Baldovi, S. Navalon, Hybrid sp2/sp3 nanodiamonds as heterogeneous metal-free ozonation catalysts in water, Appl. Catal. B Environ. 299 (2021) 120673.
[20] F. Bernat-Quesada, J.C. Espinosa, V. Barbera, M. Alvaro, M. Galimberti, S. Navalon, H. Garcia, Catalytic ozonation using edge-hydroxylated graphite-based materials, ACS Sustain. Chem. Eng. 7 (2019) 17443–17452.
[21] A. López-Francés, F. Bernat-Quesada, M. Cabrero-Antonino, B. Ferrer, A. Dhakshinamoorthy, H.G. Baldoví, S. Navalón, Nanographite: a highly active and durable metal-free ozonation catalyst with application in natural waters, Appl. Catal. B Environ. (2023) 122924.
[22] S. Navalon, M. Alvaro, H. Garcia, Heterogeneous Fenton catalysts based on clays, silicas and zeolites, Appl. Catal. B Environ. 99 (2010) 1–26.
[23] P.C.C. Faria, J.J.M. Órfão, M.F.R. Pereira, Activated carbon catalytic ozonation of oxamic and oxalic acids, Appl. Catal. B Environ. 79 (2008) 237–243.
[24] F.J. Beltrán, F.J. Rivas, R. Montero-de-Espinosa, Catalytic ozonation of oxalic acid in an aqueous TiO2 slurry reactor, Appl. Catal. B Environ. 39 (2002) 221–231.
[25] M. Sui, L. Sheng, K. Lu, F. Tian, FeOOH catalytic ozonation of oxalic acid and the effect of phosphate binding on its catalytic activity, Appl. Catal. B Environ. 96 (2010) 94–100.
[26] F.J. Beltrán, F.J. Rivas, R. Montero-de-Espinosa, Ozone-enhanced oxidation of oxalic acid in water with cobalt catalysts. 1. Homogeneous catalytic ozonation, Ind. Eng. Chem. Res. 42 (2003) 3210–3217.
[27] C. Saka, Metal-free hybrid composite particles with phosphorus and oxygen-doped graphitic carbon nitride dispersed on kaolin for catalytic activity toward efficient hydrogen release, Int. J. Hydrogen Energy 48 (2023) 13864–13876.
[28] C. Saka, Highly active hydrogen generation from sodium borohydride methanolysis and ethylene glycolysis reactions using protonated chitosan-zeolite hybrid metal-free particles, Appl. Catal. B Environ. 325 (2023) 122335.
[29] C. Saka, Metal-free phosphorus and boron-doped graphitic carbon nitride/zeolite hetero-linked particles for highly efficient green hydrogen production in methanol, Environ. Sci. Pollut. Res. Int. 30 (2023) 43480–43495.
[30] C. Saka, Surface modification strategies for nanoparticles based on chitosan and titanium dioxide: catalytic properties and mechanism for sodium borohydride dehydrogenation in methanol, Fuel 356 (2024) 129552.
[31] C. Saka, Facile oxygen doped heterojunction structured hybrid particles with γ-aluminium oxide dispersed over graphitic carbon nitride for dehydrogenation of sodium borohydride in methanol: catalytic properties and mechanism, Int. J. Hydrogen Energy 51 (2024) 1089–1098.
[32] Y. Wang, Y. Wang, Y. Wang, X. Duan, Y. Xie, H. Sun, S. Wang, Nanocarbon-based catalytic ozonation for aqueous oxidation: engineering defects for active sites and tunable reaction pathways, ACS Catal. 10 (2020) 13383–13414.
[33] A. Lopez-Frances, M. Cabrero-Antonino, F. Bernat-Quesada, B. Ferrer, M. Blanes, R. Garcia, P. Almenar, M. Alvaro, A. Dhakshinamoorthy, H.G. Baldovi, S. Navalon, Valorization of field-spent granular activated carbon as heterogeneous ozonation catalyst for water treatment, ChemSusChem (2024) e202400062.
[34] S. Navalon, A. Dhakshinamoorthy, M. Alvaro, H. Garcia, Carbocatalysis by graphene-based materials, Chem. Rev. 114 (2014) 6179–6212.
[35] X. Duan, H. Sun, S. Wang, Metal-free carbocatalysis in advanced oxidation reactions, Acc. Chem. Res. 51 (2018) 678–687.
[36] D.S. Su, G. Wen, S. Wu, F. Peng, R. Schlögl, Carbocatalysis in liquid-phase reactions, Angew. Chem. Int. Ed. 56 (2017) 936–964.
[37] M. Antonietti, N. Lopez-Salas, A. Primo, Adjusting the structure and electronic properties of carbons for metal-free carbocatalysis of organic transformations, Adv. Mater. 31 (2019) 1805719.
[38] P.M. Alvárez', F.J. Beltrán, F.J. Masa, J.P. Pocostales, A comparison between catalytic ozonation and activated carbon adsorption/ozone-regeneration processes for wastewater treatment, Appl. Catal. B Environ. 92 (2009) 393–400.
[39] P.M. Alvárez, J.F. García-Araya, F.J. Beltrán, I. Giráldez, J. Jaramillo, V. Gómez-Serrano, The influence of various factors on aqueous ozone decomposition by granular activated carbons and the development of a mechanistic approach, Carbon 44 (2006) 3102–3112.
[40] Y. Wang, H. Cao, L. Chen, C. Chen, X. Duan, Y. Xie, W. Song, H. Sun, S. Wang, Tailored synthesis of active reduced graphene oxides from waste graphite: structural defects and pollutant-dependent reactive radicals in aqueous organics decontamination, Appl. Catal. B Environ. 229 (2018) 71–80.
[41] A.G. Gonçalves, J.L. Figueiredo, J.J.M. Órfão, M.F.R. Pereira, Influence of the surface chemistry of multi-walled carbon nanotubes on their activity as ozonation catalysts, Carbon 48 (2010) 4369–4381.
[42] J. Restivo, C.A. Orge, A.S. Guedes Gorito dos Santos, O.S.G.P. Soares, M.F. R. Pereira, Nanostructured layers of mechanically processed multiwalled carbon nanotubes for catalytic ozonation of organic pollutants, ACS Appl. Nano Mater. 3 (2020) 5271–5284.
[43] L. Peng, Y. Peng, A. Primo, H. García, Porous graphitic carbons containing nitrogen by structuration of chitosan with pluronic P123, ACS Appl. Mater. Interfaces 13 (2021) 13499–13507.
[44] M. Trandafir, M. Florea, F. Neaţu, A. Primo, V.I. Parvulescu, H. García, Graphene from alginate pyrolysis as a metal-free catalyst for hydrogenation of nitro compounds, ChemSusChem 9 (2016) 1565–1569.
[45] L. Peng, A. Doménech-Carbó, A. Primo, H. García, 3D defective graphenes with subnanometric porosity obtained by soft-templating following zeolite procedures, Nanoscale Adv. 1 (2019) 4827–4833.
[46] A. Dhakshinamoorthy, M.A. Latorre-Sanchez, M. A, A. Primo, H. Garcia, Sulphur-doped graphene as metal-free carbocatalysts for the solventless aerobic oxidation of styrenes, Catal. Commun. 65 (2015) 10–13.
[47] I.K.M. Yu, X. Xiong, D.C.W. Tsang, Y.H. Ng, J.H. Clark, J. Fan, S. Zhang, C. Hu, Y. S. Ok, Graphite oxide- and graphene oxide-supported catalysts for microwave-assisted glucose isomerisation in water, Green Chem. 21 (2019) 4341–4353.
[48] B. Kasprzyk-Hordern, M. Ziółek, J. Nawrocki, Catalytic ozonation and methods of enhancing molecular ozone reactions in water treatment, Appl. Catal. B Environ. 46 (2003) 639–669.
[49] S. Psaltou, E. Kaprara, K. Triantafyllidis, M. Mitrakas, A. Zouboulis, Heterogeneous catalytic ozonation: the significant contribution of PZC value and wettability of the catalysts, J. Environ. Chem. Eng. 9 (2021) 106173.
[50] S. Psaltou, M. Mitrakas, A. Zouboulis, Heterogeneous catalytic ozonation: solution pH and initial concentration of pollutants as two important factors for the removal of micropollutants from water, Separations 9 (2022) 413.
[51] Y. Dadban Shahamat, M. Sadeghi, A. Shahryari, N. Okhovat, F. Bahrami Asl, M. M. Baneshi, Heterogeneous catalytic ozonation of 2, 4-dinitrophenol in aqueous solution by magnetic carbonaceous nanocomposite: catalytic activity and mechanism, Desalination Water Treat. 57 (2015) 20447–20456.
[52] Y. Liu, J. Zhao, Z. Li, G. Li, W. Li, X. Gao, Catalytic ozonation of bisphenol A in aqueous solution using Mn-Ce/HZSM-5 as catalyst, Water Sci. Technol. 72 (2015) 696–703.
[53] J.L. Figueiredo, M.F.R. Pereira, M.M.A. Freitas, J.J.M. Órfão, Modification of the surface chemistry of activated carbons, Carbon 37 (1999) 1379–1389.
[54] J.C. Espinosa, P. Manickam-Periyaraman, F. Bernat-Quesada, S. Sivanesan, M. Álvaro, H. Garcia, S. Navalon, Engineering of activated carbon surface to enhance the catalytic activity of supported cobalt oxide nanoparticles in peroxymonosulfate activation, Appl. Catal. B Environ. 249 (2019) 42–53.
[55] Y. Wang, Y. Xie, H. Sun, J. Xiao, H. Cao, S. Wang, Efficient catalytic ozonation over reduced graphene oxide for p-hydroxylbenzoic acid (PHBA) destruction: active site and mechanism, ACS Appl. Mater. Interfaces 8 (2016) 9710–9720.
[56] S. Song, M. Wang, Z. Wang, Y. Wang, R. Li, Y. Zhang, C. Liu, Y. Liu, B. Xu, F. Qi, Insights into heteroatom-doped graphene for catalytic ozonation: active centers, reactive oxygen species evolution, and catalytic mechanism, Environ. Sci. Technol. 53 (2019) 5337–5348.
[57] Y. Wang, H. Cao, L. Chen, C. Chen, X. Duan, Y. Xie, W. Song, H. Sune, S. Wang, Tailored synthesis of active reduced graphene oxides from waste graphite: structural defects and pollutant-dependent reactive radicals in aqueous organics decontamination, Appl. Catal. B Environ. 229 (2018) 71–80.

[58] Y. Wang, H. Cao, H. Chen, Y. Xie, H. Sun, X. Duan, S. Wang, Metal-free catalytic ozonation on surface-engineered graphene: microwave reduction and heteroatom doping, Chem. Eng. J. 355 (2019) 118–129.
[59] S.R.M. Plimpton, D. G, C. Austin, S.S. Eaton, G.R.G. Eaton, G. C, M. Voskuil, Remote delivery of hydroxyl radicals via secondary chemistry of a nonthermal plasma effluent, Biotechnol. Bioeng. 110 (2013) 1936–1944.
[60] P. Bilski, K. Reszka, M. Bilska, C.F. Chignell, Oxidation of the spin trap 5,5-dimethyl-1-pyrroline n-oxide by singlet oxygen in aqueous solution, J. Am. Chem. Soc. 118 (1996) 1330–1338.
[61] J. Marcon, G. Mortha, N. Marlin, F. Molton, C. Duboc, A. Burnet, New insights into the decomposition mechanism of chlorine dioxide at alkaline pH, Holzforschung 71 (2017) 599–610.
[62] U. von Gunten, Ozonation of drinking water: part I. Oxidation kinetics and product formation, Water Res. 37 (2003) 1443–1467.
[63] N. Miyoshia, M. Uedaa, K. Fukeb, Y. Tanimotoa, M. Itoha, G. Tomitac, Lifetime of singlet oxygen and quenching by NaN3 in mixed solvents, Z. Naturforsch. 37b (1982) 649–652.
[64] E.L. Clennan, Aromatic endoperoxides, Photochem. Photobiol. 99 (2023) 204–220.
[65] H. Fidder, A. Lauer, W. Freyer, B. Koeppe, K. Heyne, Photochemistry of anthracene-9,10-endoperoxide, J. Phys. Chem. A 113 (2009) 6289–6296.